JOURNAL OF PROPULSION AND POWER
Vol. 19, No. 3, May–June 2003

Technical Notes

TECHNICAL NOTES are short manuscripts describing new developments or important results of a preliminary nature. These Notes cannot exceed 6 manuscript pages and 3 figures; a page of text may be substituted for a figure and vice versa. After informal review by the editors, they may be published within a few months of the date of receipt. Style requirements are the same as for regular contributions (see inside back cover).

Analysis of Entrainment in a Sudden-Expansion Channel with Wall Mass Transfer

Jing-Tang Yang* and Shih-Chao Lee†
National Tsing Hua University,
Hsinchu 300, Taiwan, Republic of China
and
Yei-Chin Chao‡
National Cheng-Kung University,
Tainan 701, Taiwan, Republic of China

Introduction

TO model the pyrolysis phenomena in a solid fuel ramjet-based system, one of the common methods is to inject mass from a porous plate following a sudden expansion channel. Earlier studies[1–3] indicate that such a flowfield possesses the features of inlet mainstream, shear layer, primary and secondary recirculation bubbles, and redeveloped boundary layer. The flow structure is shown schematically in Fig. 1. To find the interactions among these structures just mentioned, Ma[3] experimented and reported that there existed four distinct flow patterns formed in almost the same flow region by varying the mass flow ratio between the injection and the mainstream. Pattern A is the well-known backstep flow without wall injection that includes all of the structures depicted in Fig. 1. With the addition of mass injection, the observed major flow structures of pattern B are the same with those of pattern A, except that the main recirculation bubble is smaller than that of pattern A because of the squeeze of the expanded corner eddy. The primary recirculation bubble is squashed by the inlet flow concurrently with wall injection in pattern C, in which a small counterclockwise rotating eddy appears at the front of the depressed recirculation bubble. For pattern D all of the structures depicted in Fig. 1 are destroyed by a certainly high wall mass ratio. In an SFRJ the most important goal is to enlarge the primary recirculation bubble to entrain additional fresh air to stable the flame . Nonetheless, Pitz and Daily[4] showed that a combustion separated flow would exhibit a reattachment length 30% shorter than that of the nonreaction cold flow. The main objective reached here is to explore further the influences of wall mass injection on the recirculation structure and entrainment for an SFRJ-based system. Because the absence of the detailed flow features from the measurements, accurate numerical simulation provides an alternative way to examine more, spatially and temporally, physical insights. In large eddy simulations (LES) large energy-carrying eddies, usually significantly larger than the fine grid size, are directly computed in detail so that their structural evolution and dynamic behavior, such as the dynamic vortical evolution and entrainment, can be resolved, and only the small subgrid ones are modeled. The present work thus uses a LES that coordinates with new near-wall treatments to investigate the effects just mentioned, particularly addressing a close relationship between the reverse strength and entrainment upstream of the reattachment point.

Numerical Solver

The elliptic transport equations that include the continuity, stream-wise, and transverse momentums, and mass transfer govern the entire flow region, as shown in Fig. 1. On a Cartesian staggered grid system with refined meshes close to walls and shear layer, the full set of discretized transport equations that consists of the diffusion and convective terms respectively is derived by central differencing. The QUICK[5] scheme is solved via a line-by-line tridiagonal-matrix algorithm, whereas the Crank–Nicolson scheme is adopted to ensure time-marching stability. The pressure solver is a SIMPLE[6] algorithm. All of the initial and boundary conditions are compiled from the measurements of Ma.[3] The lateral boundary is modified to approach Stokes flow inside the porous plate. Close to this upper side, a new near-wall model is also applied to avoid employing redundant grid. For further details of the present simulation procedure and analysis, see Ref. 7.

Results and Discussion

The test conditions of this work are based on the measurements of Ma.[3] A sudden expansion channel of total length 160 cm with a porous plate (30 cm in length and 20 cm in width) behind the step (1.5 cm height) constitutes the experimental geometric configuration, whereas the height of inlet channel is 3 cm. Based on the step height H, the corresponding inlet Reynolds numbers are all below 3×10^3. The maximal wall mass ratio and the pressure drop across the porous plate are about 0.081 and 2 kPa, respectively. The dimensionless reverse rate is defined as Q_r / Q_{in}, in which

$$Q_r = -\int_0^{y_*} u \, dy, \qquad Q_{\text{in}} = 2U_0 H + v_w L$$

where y_* corresponds to the point of zero horizontal velocity with negative streamwise velocity between $y = 0$ and y_* and L represents the length of porous plate. Both results of the numerical evaluation and the experimental data are consistent and reveal that the strongest reversal rates occurs approximately from $0.45x_r$ to $0.6x_r$ for all cases

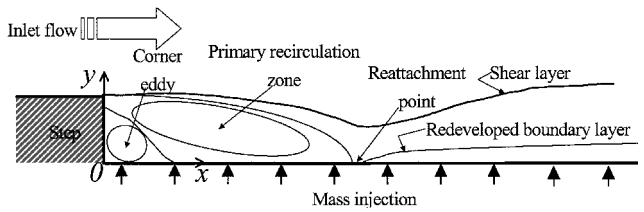

Fig. 1 Schematic of backward-facing step showing geometric and flow configurations.

Received 29 April 2002; revision received 23 August 2002; accepted for publication 30 August 2002.

*Professor, Department of Power Mechanical Engineering; jtyang@pme.nthu.edu.tw.
†Ph.D., Department of Power Mechanical Engineering.
‡Professor, Department of Aeronautics and Astronautics; ycchao@mail.ncku.edu.tw. Member AIAA.

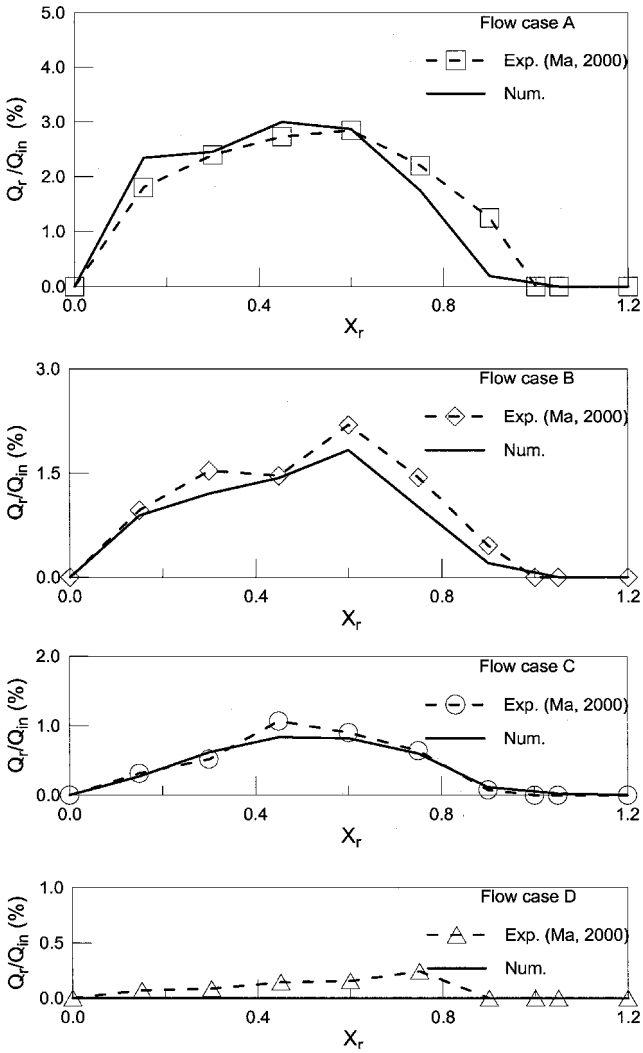

Fig. 2 Distributions of dimensionless reverse flow rate along horizontal direction for different flow cases.

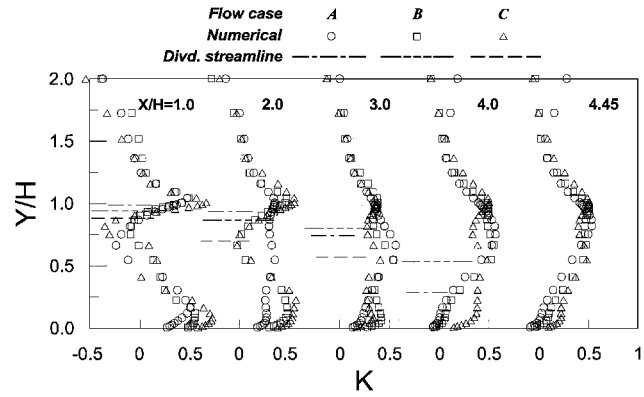

Fig. 3 Profiles of shear correlation coefficient at stations $x/H = 1.0, 2.0, 3.0, 4.0$, and 4.45 for flow cases A, B, and C.

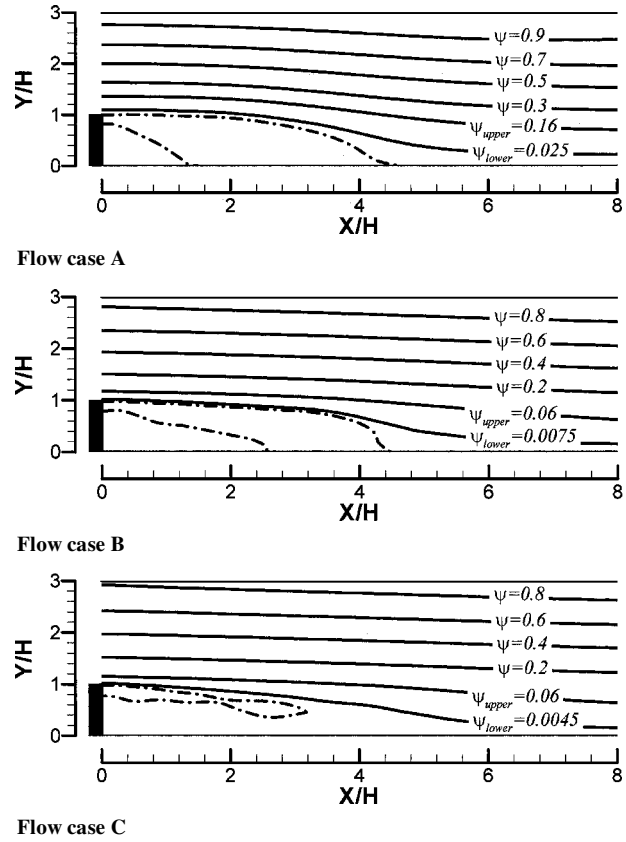

Fig. 4 Lines of dimensionless stream function: – · –, dividing streamline ($\psi = 0$).

A, B, and C, in Fig. 2. For the case without wall injection, about 15.63% of the new shear layer is deflected upstream the reattachment point, whereas approximately 12.5 and 7.5% of the new shear layer is deflected upstream for the flowfields B and C, respectively. The corresponding maximal Q_r/Q_{in} for the cases A, B, and C are 2.99, 1.83, and 0.84%, respectively. Because the primary recirculation zone is entirely destroyed in case D, the analysis is not conducted further in this work.

According to the concept of Etheridge and Kemp,[8] an analysis, based upon the dimensionless stream function

$$\psi = \int_0^y \frac{u\,\mathrm{d}y}{Q_{\text{in}}} \qquad (y = 0 \sim 3H)$$

and the shear correlation coefficient $K = -\overline{u'v'}/\sqrt{\overline{u'u'}\,\overline{v'v'}}$, is performed to investigate the mixing between the main stream and the recirculation zone that occurs upstream of the reattachment point. On these bases the development of the shear layer upstream of the reattachment point for different flow patterns of the present simulation can be demonstrated in Figs. 3 and 4. All of the K profiles exhibit a positive peak near the dividing streamlines of these patterns at the stations $x/H = 1.0$ and 2.0. These peaks occur apart at $x/H = 3.0$, but become concentrated at $x/H = 4.0$ and almost converge toward a single curve at $x/H = 4.45$ with relative flatter regions in $y/H = 0.5 \sim 0.95$.

The sharp peaks of the K profiles are reasonably regarded as the upper boundaries of the shear layer.[8] The corresponding K of the upper boundaries in cases A, B, and C are thus respectively 0.53, 0.50, and 0.48 (Fig. 3), which respectively corresponds to $\psi_{\text{upper}} = 0.16$, 0.06, and 0.06 (Fig. 4). Although the distributions of K within the shear layer are not all in perfect uniform, the lower bounds of the shear layers are estimated from Figs. 3 and 4 to be $K = 0.53$, 0.50, 0.48, and $\psi_{\text{lower}} = 0.025$, 0.0075, and 0.0045, respectively corresponding to cases A, B, and C. Most of the fluid beneath the streamline ψ_{lower} likely flows in the reverse direction toward the step, and the amount of the maximal entrainment is equal to the stream function ψ_{lower}.

The other interesting parameters $Q_{\text{inj\_rez/2}}$, $Q_{r\_\max}$, and ΔQ are further estimated and listed in Table 1 in attempt to correlate the relation among the wall mass injected in the rear part of the reattachment length, the maximal reverse strength, and the difference between the maximal reverse flux and the entrainment flux. Because the maximal reverse flow rates for the cases A, B, and C are approximately

Table 1 Numerical test conditions and the ratios of predicted flow rates

Flow case	$\frac{v_w}{U_0}$	ψ_{lower}[a]	ψ_{upper}[b]	$\frac{Q_{\text{inj\_rez}/2}}{Q_{\text{in}}}$[c]	$\frac{\psi_{\text{lower}}}{\psi_{\text{upper}}}$[d]	$\frac{Q_{r\_\max}}{Q_{\text{in}}}$[e]	$\frac{\Delta Q}{Q_{\text{inj\_rez}/2}}$[f]
A	0	2.50%	16.0%	0	15.63%	2.99%	——
B	1.47%	0.75%	6.0%	1.43%	12.50%	1.83%	75.55%
C	2.05%	0.45%	6.0%	1.89%	7.50%	0.84%	20.61%
D	7.87%	——	——	4.90%	——	——	——

[a] Stream function at the lower boundary of the new shear layer.
[b] Stream function at the upper boundary of the new shear layer.
[c] $Q_{\text{inj\_rez}/2}$-half-injection rate within the region of 4.45 times of step height.
[d] Percentage of the new shear layer deflected upstream the reattachment point.
[e] $Q_{r\_\max}$-maximal reverse flow rate.
[f] $\Delta Q = Q_{r\_\max} - \psi_{\text{lower}} Q_{\text{in}}$.

located at $0.5x_r$, the present choice of $\Delta Q/Q_{\text{inj\_rez}/2}$ conveniently gives the wall injection that most probably contributes to the maximal strength of reversal flow. For case A, without mass injection, the entrainment is less than 2.5% of the total inflow rate, which is very close to the maximal reverse flow rate in the recirculating zone. For cases B and C the more the mass is injected from the wall, the less the entrainment and maximal reverse flow rate becomes. This trend is clearly related to both the enlargement of the corner eddy and the lift of the main recirculating bubble from the porous wall. About 75.55% of the injected mass can contribute to the maximal reverse flow in case B, whereas only 20.61% in case C. All of these phenomena are beneficial to the analysis of the ignition in SFRJ-based systems or transpiration cooling in separated flows.

Conclusions

This study investigates numerically the effects of lateral injection rate on the inlet mainstream that deflects the reattachment point upstream with special focus on the intimately relation between the maximal reverse rate and the entrainment fluid. The analysis reveals that the enhancement of blowing rate suppresses apparently the strongest reversal strength because of the enlargement of the corner eddy and the lift of the main recirculating bubble from the porous wall. For the case without wall injection, about 15.63% of the new shear layer is deflected upstream the reattachment point, whereas approximately 12.5 and 7.5% of the new shear layer are deflected upstream for the flow fields B and C, respectively.

References

[1] Yang, J. T., Tsai, B. B., and Tsai, G. L., "Separated-Reattaching Flow over a Backstep with Uniform Normal Mass Bleed," *Journal of Fluids Engineering*, Vol. 116, No. 1, 1994, pp. 29–35.

[2] Richardson, J., de Groot, W. A., Jadoga, J. I., Walterick, R. E., Hubbartt, J. E., and Strahle, W. C., "Solid Fuel Ramjet Simulator Results: Experiment and Analysis in Cold Flow," *Journal of Propulsion and Power*, Vol. 1, No. 6, 1985, pp. 488–493.

[3] Ma, W. J., "Transpiration Cooling Phenomena in Separated Flow Field," Ph.D. Dissertation, Dept. of Power Mechanical Engineering, National Tsing Hua Univ., Taiwan, June 2000.

[4] Pitz, R. W., and Daily, W., "Combustion in a Turbulent Mixing Layer Formed at a Rearward-Facing Step," *AIAA Journal*, Vol. 21, No. 11, 1983, pp. 1565–1570.

[5] Leonard, B. P., "A Stable Accurate Convective Modelling Procedure Based on Quadratic Upstream Interpolation," *Computers Method in Applied Mechanics and Engineering*, Vol. 19, No. 1, 1979, pp. 59–98.

[6] Patankar, S. V., *Numerical Heat Transfer and Fluid Flow*, Hemisphere, Washington, DC, 1980, pp. 79–138.

[7] Lee, S. C., "Structural and Mixing Characteristics of a Backstep Flow with Lateral Mass Injection Using LES with Near-Wall Treatment," Ph.D. Dissertation, Dept. of Power Mechanical Engineering, National Tsing Hua Univ., Taiwan, Nov. 2002.

[8] Etheridge, D. W., and Kemp, P. H., "Measurements of Turbulent Flow Downstream of a Rearward-Facing Step," *Journal of Fluid Mechanics*, Vol. 86, No. 3, 1978, pp. 545–566.

Leading-Edge Shape and Aeroengine Fan Blade Performance

A. I. Sayma* and M. Kim†
Imperial College,
London, England SW7 2BX, United Kingdom
and
N. H. S. Smith‡
Rolls–Royce plc.,
Derby, England DE24 8BJ, United Kingdom

Introduction

DURING ascent and descent, an aircraft often passes through clouds consisting of water and dirt particles, which impinge on, and erode, the leading edge of fan blades. Overall, the level of erosion increases with blade radius as the relative inlet Mach number increases. The tip region of the fan blades experiences less erosion because the nacelle offers some protection. Theoretical analysis of a bluff profile shows that locally increased accelerations around the leading edge relative to a semicircular profile result in increased shock and profile loss. In practice, this loss of efficiency due to erosion can be recouped through systematic redressing of the fan blades during scheduled servicing and overhaul.

To predict the effects of leading-edge shape on performance, the numerical prediction tools must capture the complexity of the flow near the leading edge, where high-velocity gradients and boundary-layer flow transition are observed. Some methods are now being tested for performance evaluations of more realistic geometry definitions as found during extended service operation, for example, a blunt-nosed aerofoil shape, or for performance changes resulting from surface coatings/roughness, as reported by Suder et al.[1] However, with the absence of reliable and standard transition prediction tools, the problem is a formidable challenge, and this explains why researchers have generally refrained from attempting such predictions.

This Technical Note concentrates on two aspects of the preceding discussion. First, it will be shown that overall performance and stability margin changes can be captured, without excessively fine grids or transition models, for small geometric leading-edge differences. Second, an attempt will be made to explain the underlying physical mechanisms that cause flutter margin changes.

Overview of the Numerical Methodology

The results are obtained with a well-established unsteady aeroelasticity code whose aerodynamic part is an edge-based upwind solver.[2] The time stepping is implicit; hence, large Courant–Friedrichs–Lewy numbers can be used without creating numerical instabilities. Time accuracy is ensured by a dual-time stepping technique. The code solves the Reynolds averaged Navier–Stokes equations with Baldwin–Barth, Spalart–Allmaras one-equation, or q–ζ two-equation turbulence models. The flow geometry is described using a mixture of tetrahedra, hexahedra, and wedge elements. The structural part uses a modal model obtained from a three-dimensional finite element representation.[3] The structural

Received 28 May 2002; revision received 9 December 2002; accepted for publication 30 January 2003.

*Rolls–Royce Research Fellow, Mechanical Engineering. Member of the Royal Aeronautical Society.
†Research Assistant, Centre of Vibration Engineering, Mechanical Engineering Department.
‡Staff Technologist, Fan Systems.